Shap. Mem. Superelasticity (2016) 2:37–49
DOI 10.1007/s40830-015-0049-5

Cyclic Degradation of $Co_{49}Ni_{21}Ga_{30}$ High-Temperature Shape Memory Alloy: On the Roles of Dislocation Activity and Chemical Order

P. Krooß[1] · P. M. Kadletz[2] · C. Somsen[3] · M. J. Gutmann[4] · Y. I. Chumlyakov[5] · W. W. Schmahl[2] · H. J. Maier[6,7] · T. Niendorf[1]

Published online: 30 December 2015

Abstract Conventional shape memory alloys (SMAs), such as binary Ni–Ti, are typically limited to service temperatures below 100 °C. Recent studies on Co–Ni–Ga high-temperature SMAs revealed the potential that these alloys can be used up to temperatures of about 400 °C. Analysis of the cyclic functional properties showed that degradation in these alloys is mainly triggered by intensive dislocation motion. However, data on the cyclic stress–strain response and the mechanisms leading to functional degradation of Co–Ni–Ga above 300 °C were missing in open literature. Current results reveal that above 300 °C diffusion-controlled mechanisms, e.g., precipitation of secondary phases and changes in the chemical degree of order, seem to dictate cyclic instability. Detailed neutron and transmission electron microscopy analyses following superelastic cycling in a temperature range of 200–400 °C were employed to characterize the changes in degradation behavior above 300 °C.

Keywords Shape memory alloy (SMA) · Martensitic phase transformation · Functional degradation · Martensite stabilization · Superelasticity

This article is an invited paper selected from presentations at the International Conference on High-Temperature Shape Memory Alloys 2015, held May 5–8, 2015, in Wildbad Kreuth Educational Centre in Kreuth, Bavaria, Germany, and has been expanded from the original presentation.

✉ T. Niendorf
niendorf@uni-kassel.de

[1] Institut für Werkstofftechnik, Universität Kassel, 34125 Kassel, Germany

[2] Applied Crystallography, Department of Earth and Environmental Sciences, Ludwig-Maximilians-Universität, 80333 Munich, Germany

[3] Institut für Werkstoffe, Ruhr-Universität Bochum, 44801 Bochum, Germany

[4] Rutherford Appleton Laboratory, ISIS Facility, Chilton Didcot, Oxfordshire OX11 0QX, UK

[5] Siberian Physical Technical Institute, Tomsk State University, Novosobornay Square 1, Tomsk, Russia 634050

[6] Institut für Werkstoffkunde (Materials Science), Leibniz Universität Hannover, 30823 Garbsen, Germany

[7] Zentrum für Festkörperchemie und Neue Materialien, Leibniz Universität Hannover, 30167 Hannover, Germany

Introduction

Shape memory alloys (SMAs) have been studied intensively in the last decades [1–5]. They are promising candidates for actuation and damping applications due to their unique material properties [1–4]. Based on a thermoelastic martensitic phase transformation from a high-temperature austenitic phase to a low-temperature martensitic phase high reversible transformation strains can be obtained [1–5]. Conventional binary Ni–Ti alloys exhibit fully reversible transformation strains of about 10 %, but the effect is limited to service temperatures of about 100 °C [2]. Above this temperature plastic deformation sets in [1–5]. While processing of conventional Ni-based SMAs is quite costly, newly developed Fe-based SMAs such as Fe–Ni–Co–Al–Ta and Fe–Mn–Al–Ni show significantly improved processability, similar transformation strains, but remarkably lower transformation temperatures [6, 7]. In order to extend the operating temperature range beyond 100 °C, numerous high-temperature (HT) SMAs, such as Ti–Ta–X (X = Al, Zr) [2, 8, 9], Ni–Ti–X (X = Pd, Pt, Hf, Zr) [10–14], and Co–Ni–X (X = Ga, Al) [2, 8–22] have been developed. Most

HT-SMAs suffer from pronounced brittleness, e.g., Ni–Ti–Hf, Ni–Ti–Zr, and high costs for alloying elements, e.g., Ni–Ti–Pd, Ni–Ti–Pt, making processing of these alloys in bulk very difficult or markedly cost inefficient [10–14, 23–25]. The recently proposed binary and ternary Ti-based systems, Ti–Ta and Ti–Ta–Al, show promising properties, i.e., high transformation temperatures and high ductility allowing for cold deformation up to 90 % in combination with lower costs for the alloying elements [2, 8, 9]. However, these alloys suffer from functional degradation induced by multiple mechanisms, i.e., increased dislocation activity and diffusion-controlled precipitation. While high heating–cooling rates led to dislocation dominated functional degradation in the course of cycling, slow heating–cooling rates, i.e., longer dwell times in critical temperature regimes, resulted in diffusion-controlled functional degradation [26–28]. For a more detailed overview of HT-SMAs in general, the reader is referred to a review published by Ma et al. [2].

Co–Ni–Ga HT-SMAs are promising candidates for high-temperature damping and actuation applications since these exhibit superelasticity and shape memory behavior in a temperature range up to 400 °C [29, 30]. Processing of polycrystalline Co–Ni–Ga materials can be significantly improved by the precipitation of the disordered secondary γ-phase (A1), which makes the alloy distinctly better workable than its counterpart, Co–Ni–Al [18]. In general, Co–Ni–Ga SMAs are characterized by a thermoelastic martensitic transformation from a high-temperature cubic B2-ordered parent phase to a tetragonal low-temperature martensitic phase with an $L1_0$ structure [31]. Co–Ni–Ga HT-SMAs have been intensively investigated in recent years [15–17, 19–22, 29–31]. Dadda et al. analyzed the transformation characteristics under compression in both, single cycle tests and fatigue experiments at room temperature [15–17]. The focus in these studies was the evolution of transformation strains and characterization of suitable superelastic temperature regimes for different crystallographic orientations after various training and aging procedures of the single crystalline material [15–17]. Later, Monroe et al. focused on the development of the superelastic performance under tensile loads at various temperatures [22].

Due to a lack of data in the open literature reporting on fatigue mechanisms at higher temperatures, the current authors recently addressed the tension–compression asymmetry and discussed the degradation mechanisms dictating functional instability up to 300 °C using transmission electron microscopy (TEM) and neutron diffraction analysis [30]. The results unequivocally revealed, that the degradation of the functional performance up to 300 °C, under both tensile and compressive loads, is mainly related to an enhanced dislocation formation, whereas a contribution of diffusion-controlled mechanisms, i.e., changes in the degree of chemical order, was found to be of less importance [30]. Focusing on the changes in the degree of chemical order, a recently published study reported on the effect of aging in the stress-induced martensitic (SIM) phase in Co–Ni–Ga single crystals under compression [29]. The results clearly revealed that the transformation temperatures significantly increase by about 150 °C [29] after SIM-aging for 20 min at 400 °C and for 8.5 h at 300 °C. The increase of transformation temperatures was explained based on a change of the Gibbs free energy due to a change of chemical order, which was, among others, explained by the principle of symmetry-conforming, short-range ordering (SC-SRO), proposed by Ren and Otsuka [32]. Neutron diffraction analysis was employed for experimental determination of underlying mechanisms [31]. Differing intensities of superlattice reflections were found and attributed to changes in chemical order. However, unambiguous distinction between long- and short-range ordering phenomena was not feasible, so that contribution of SC-SRO was concluded [31]. These experiments led to the assumption that changes in the degree of order might affect superelastic degradation in addition to dislocation formation and/or motion, especially at elevated temperatures in Co–Ni–Ga SMAs. For the intended industrial application, however, a better understanding of the mechanisms leading to functional degradation is crucial. Thus, the present study focuses on the impact of test temperatures on the active degradation mechanisms under superelastic tensile loading in single crystalline [001]-oriented Co–Ni–Ga up to 500 °C.

Materials and Experimental Techniques

Using vacuum induction melting, $Co_{49}Ni_{21}Ga_{30}$ (in at.%) ingots were produced. Large single crystals were grown in a He atmosphere using the Bridgman technique. Dog-bone-shaped tensile samples with a gage length of 6 mm and a cross section of 1.5 × 1.5 mm^2 were machined from the bulk material with the [001] austenite direction parallel to the loading direction. All samples were tested in the as-grown condition in order to allow for better comparison with data from literature.

The material response was evaluated at temperatures up to 500 °C in quasistatic uniaxial tensile tests using a servohydraulic test rig in displacement control at a nominal displacement rate of 5 × 10^{-4} s^{-1}. In order to characterize the superelastic cyclic stress–strain response, the samples were cycled at 400 °C. Strains were calculated from displacement data, and a reference test at room temperature employing a miniature extensometer featuring a 3 mm

gage length was employed for calibration purpose. Heating of the samples was realized by convective heating. Temperatures were measured with a thermocouple directly attached to the sample surface fixed by a steel spring.

Neutron diffraction experiments and TEM analysis were performed on both, samples tested in the present study (cycling at 400 °C) and in previous work (cycling in the temperature range from 100 to 300 °C [30]). The neutron diffraction experiments were conducted with the single crystal Laue diffractometer SXD [33] at the ISIS neutron source, Rutherford Appleton Laboratory, Oxfordshire. Using neutron diffraction the whole sample volume of several mm^3 can be probed as the attenuation length of neutrons is typically in the order of centimeter to meter and therefore larger than the attenuation length of X-rays or electrons. SXD works as a Laue camera with time-of-flight resolution employing a white beam of neutrons with incident wavelengths in the range of 0.2–10 Å. Eleven LiF/ZnS scintillator area detectors are surrounding the sample-position (further details in [33]). This setup allows to cover large 3D volumes in reciprocal space and to collect complete diffraction patterns within a relatively short time compared to constant wavelength single-crystal neutron diffractometers. Using the software SXD2001, data were indexed and integrated. Peak widths of 110 reflections on the backscattering detectors were extracted, where the resolution of $\Delta d/d$ is optimal (d being the lattice spacing). Crystal structures were plotted employing the software VESTA [34].

For microstructural analyses, an FEI Tecnai F20 transmission electron microscope operating at 200 kV was used. The TEM samples were first mechanically ground and polished down to a thickness of 0.15 mm. Finally, electron transparent areas were obtained using twin-jet polishing with a solution of 600 ml methanol, 340 ml butanol, and 60 ml perchloric acid under an applied potential of 70 V at a temperature of −25 °C.

Results

Stress–Strain Response

Figure 1 shows the results from the superelastic single cycle experiments, conducted in the temperature range from 50 to 500 °C under tension. Results reveal a perfect reversibility under these conditions. The inset in Fig. 1a shows the stress hysteresis data determined from the single cycle tests. Up to 225 °C the stress hysteresis remains relatively constant. It should be noted that data depicted in Fig. 1 were obtained from one sample subsequently heated up after each superelastic cycle. Above 200 °C the stress hysteresis increased significantly from 25 to 62 MPa at

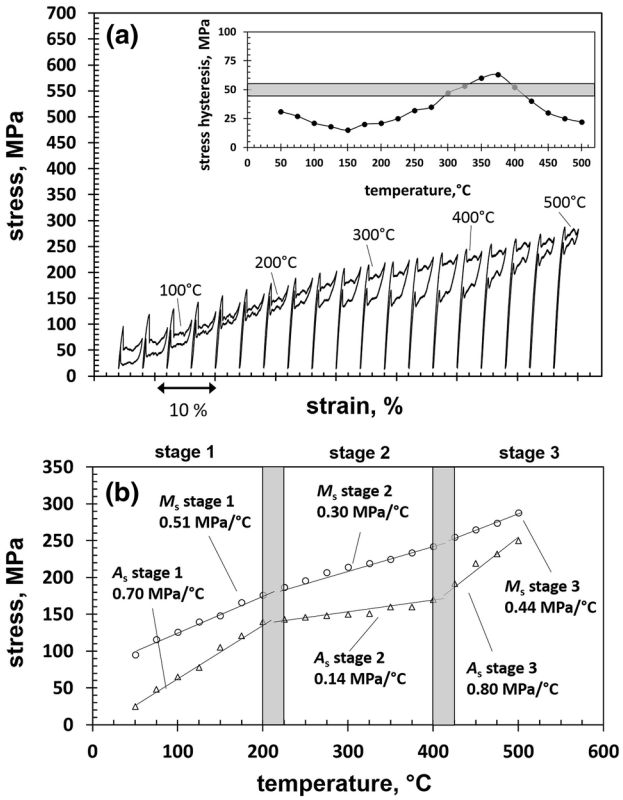

Fig. 1 Superelastic stress–strain response in an [001]-oriented Co–Ni–Ga single crystal in tension in (**a**). The *inset* in **a** depicts the stress hysteresis values of the singe cycles tests. **b** shows the M_s and A_s values obtained from the single cycles tests. All data points up to 400 °C are recompiled from [30]

375 °C. Interestingly, the stress hysteresis starts to decrease again above a temperature of about 400 °C. Whereas the evolution of the stress hysteresis was divided into two stages in the previous study [30] the current data reveal a third stage above 375 °C hinting at a significant change in the underlying microstructure evolution. As is well known, σ_{crit} values for forward and reverse transformations correlate with martensite start (M_s) and austenite start (A_s) values, respectively. Figure 1b shows the evolution of M_s and A_s extracted from the single cycle tests. Whereas the Clausius–Clapeyron (CC)-slopes for M_s and A_s remain relatively constant up to 200 °C, i.e., 0.51 and 0.70 MPa/°C, above 225 °C, the slopes change to 0.30 and 0.14 MPa/ °C up to 400 °C [30]. It is obvious that this change is more pronounced for A_s than for M_s, as has been already discussed previously [30]. Above 400 °C, however, the slope for A_s increases again to 0.80 MPa/ °C, i.e., it almost equals the initial value at low temperature.

Figure 2 shows the cyclic stress–strain response at 400 °C up to 1000 cycles. The critical stress for stress-induced martensitic transformation (σ_{crit} for SIMT) was found to be 233 MPa in the first cycle, which is very

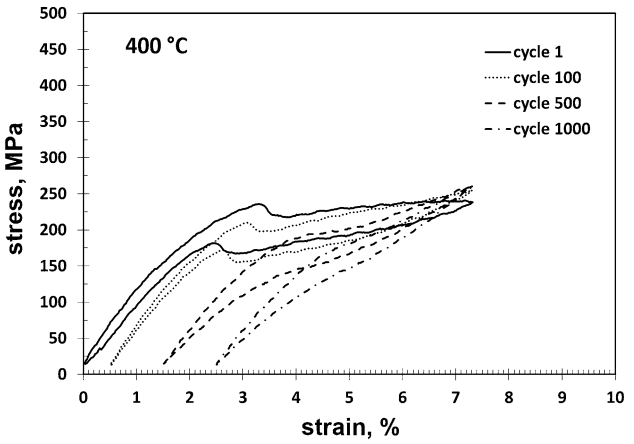

Fig. 2 Cyclic stress–strain response of [001]-oriented Co–Ni–Ga single crystals under tension at 400 °C

similar to σ_{crit} for SIMT at 300 °C in the first cycle shown previously [30]. In the following cycles σ_{crit} decreases less rapidly as compared to the tests at 300 °C [30], namely from 233 MPa in the 1st cycle to about 215 MPa in the 100th cycle and to about 195 MPa in cycle 500. Even after 1000 cycles, a martensitic transformation still is apparent, exhibiting a σ_{crit} of about 170 MPa, which indicates a clear change in the dominating degradation mechanism above 300 °C, where σ_{crit} in the 1000th cycle is only about 20 MPa. On the other hand, the accumulation of residual strain occurs more rapidly at 400 °C than at 300 °C [30]. In cycle 1000 an irrecoverable strain of about 2.5 % is apparent (Fig. 2).

For obtaining a deeper insight into the transformation behavior, distinct values of the cyclic superelastic curve were extracted as depicted in Fig. 3a, b. Data points for 100, 200 and 300 °C were recompiled from Ref. [30]. Figure 3a shows the evolution of the change in σ_{crit} for the SIMT with reference to the 1st cycle for a given test temperature. Whereas at 100 °C no change in σ_{crit} for the SIMT was observed within 1000 cycles, at 200 °C σ_{crit} decreases by about 78 MPa from the first cycle to cycle 1000. Cycling at 300 °C led to a decrease of 100 MPa already after the first 100 cycles, and σ_{crit} further decreased within the following 400 cycles to about 150 MPa. After 1000 cycles the decrease is accumulated to about 230 MPa. By contrast, for a test temperature of 400 °C the decrease in σ_{crit} is less pronounced and was found to be only about 63 MPa after 1000 cycles.

Figure 3b shows the evolution of the normalized permanent strain (ε_{nps}) as a function of cycle number. It is apparent that the increase of permanent strain is significantly higher above 300 °C than below 200 °C, where almost no residual strain is accumulated within 1000 superelastic cycles. Whereas at 300 °C the permanent strain accumulation in the first 100 cycles occurs rapidly, in the following 900 cycles an almost linear increase in the evolution of ε_{nps} is observed. At 400 °C the increase of irrecoverable strain seems to accumulate in a linear fashion immediately from the 1st to the 1000th cycle. Again, this hints at a change of the prevalent degradation mechanism.

Neutron Diffraction and Electron Microscopy

In order to provide deeper insight into the underlying mechanisms, detailed TEM and neutron diffraction analyses were conducted in various sample conditions. Figures 4a–h and 5a–c show the TEM results at RT after fatigue testing at different temperatures ranging from 200 to 400 °C. Figure 4a–d show representative TEM images depicting the microstructures resulting from superelastic cycling at distinct temperatures. The white circles represent the area where the Selected Area Electron Diffraction (SAED) patterns were taken. Figure 4e–f show the diffraction patterns for the differently fatigued conditions

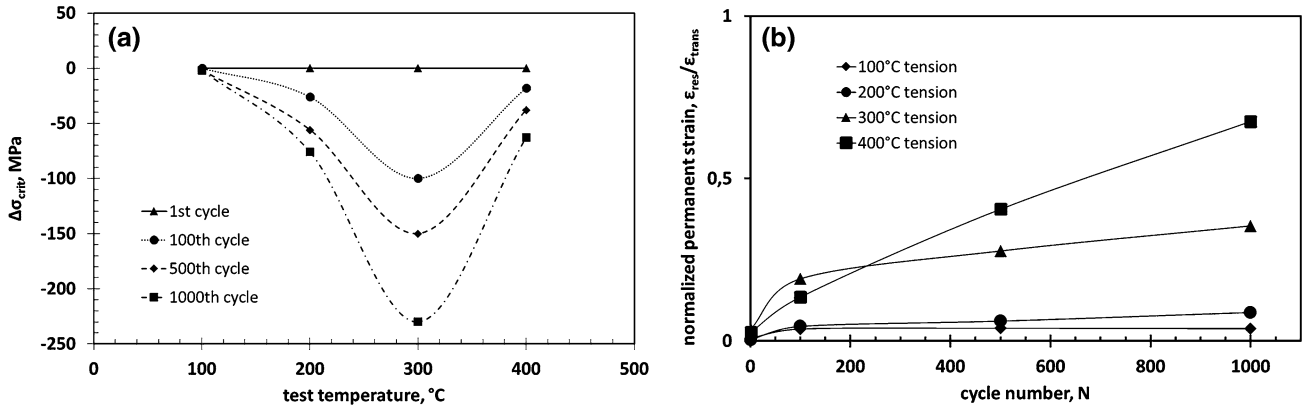

Fig. 3 Characteristic values of the cyclic stress–strain responses. The evolutions of $\Delta\sigma_{crit}$ for the 1st, 100th, 500th, and 1000th cycles are shown in **a**. **b** shows the evolution of the normalized permanent strain up to 400 °C. The data points up to 300 °C are recompiled from [30]

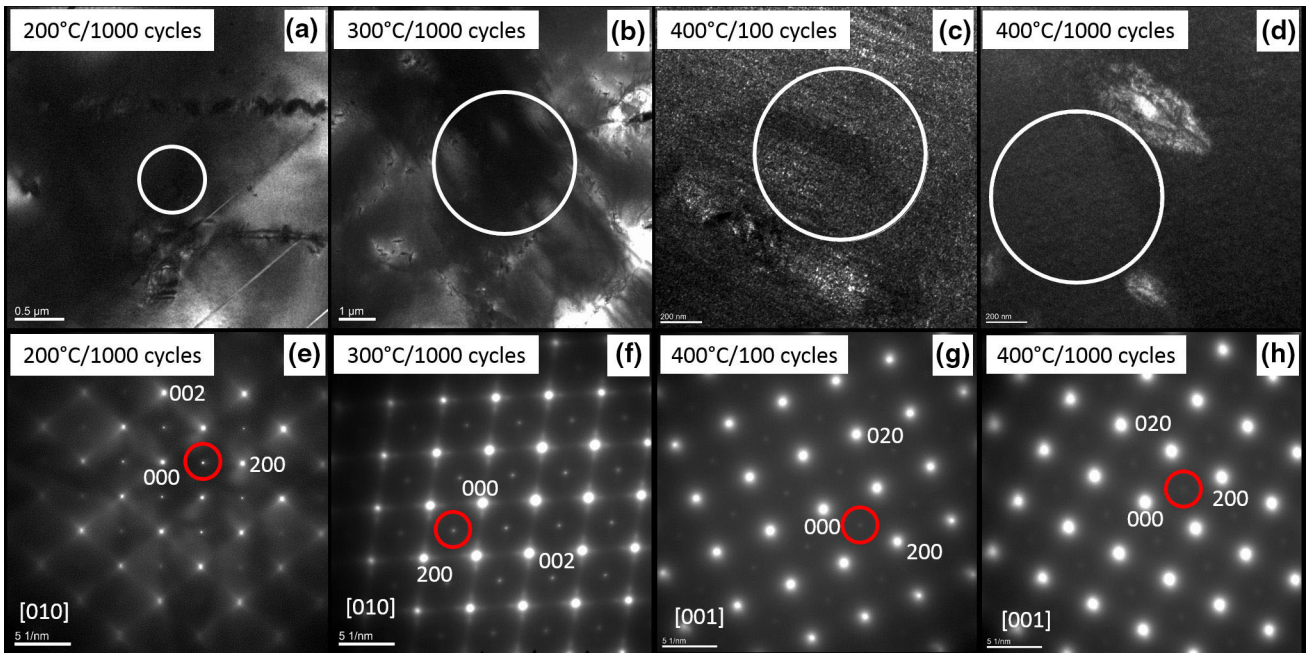

Fig. 4 TEM analysis revealing the representative microstructures present after superelastic cycling. *White circles* in the overviews in **a**–**d** indicate the areas from where the diffraction patterns in **e**–**h** were recorded. The results reveal a decreasing degree of order with increasing temperature (Color figure online)

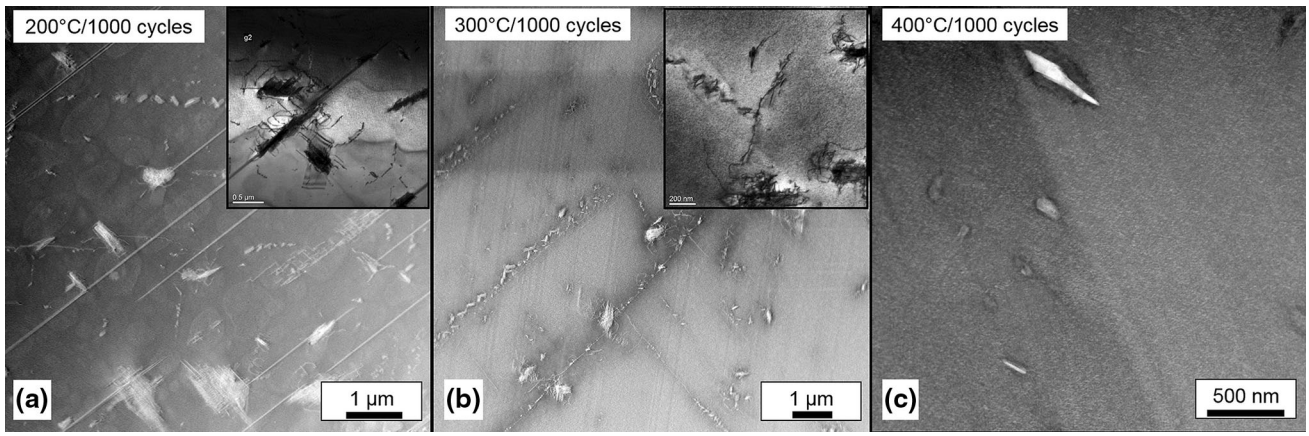

Fig. 5 TEM investigations revealing the microstructures after cycling at 200 °C for 1000 cycles in **a**, 300 °C/1000 cycles in **b,** and 400 °C/1000 cycles in **c**. The *insets* in Figures **a** and **b** show the dislocation arrangements at a higher magnification

revealing at RT that all microstructures investigated are fully martensitic after cyclic deformation at 200, 300 and 400 °C in the sample volume probed. In case of the sample cycled at 200 °C this is somewhat surprising since the superelastic hysteresis curves shown in Ref. [30] reveal a sample not being fully martensitic upon unloading following 1000 cycles. Is has to be noted that the test was stopped at 200 °C and, thus, the conclusion based on mechanical data only is valid for a temperature of 200 °C. How far cooling to room temperature affected the fraction of martensite was not evaluated in Ref. [30]. The martensitic structure was found to be ordered $L1_0$. Whereas testing at a temperature of 300 °C led to hardly any change within the $L1_0$ structure, a further increase in test temperature to 400 °C resulted in a notable change in the degree of chemical order. Definition of chemical order will be provided in the discussion section. The change in order is indicated by the change of intensity of the superlattice reflection spots of the martensitic phase marked by the red circles in Fig. 4g, h. Already after 100 cycles, the superlattice reflections seem to vanish (Fig. 4g). After 1000 cycles the degree of chemical order further decreases since

the superlattice reflections can hardly be seen anymore (Fig. 4h). This change in diffraction pattern indicates a martensite structure close to bct with a very low degree of order. As evident from Fig. 5a–c, cyclic deformation at elevated temperatures seems to have a considerable impact not only on the degree of chemical order but also on the dislocation arrangements. It is obvious from Fig. 5a–c that the microstructure changed drastically with increasing test temperature. At 200 °C twinned martensite was stabilized after 1000 superelastic cycles. The inset in Fig. 5a further reveals minor dislocation activity. After 1000 cycles at 300 °C a higher density of dislocations was found in the microstructure (Fig. 5b). An additional evaluation of the dislocation activity will be given later based on the analysis of the neutron diffraction peak width, cf. Figures 6 and 7. Figure 5b reveals that, in contrast to the TEM results for the 200 °C fatigue test (Fig. 5a), fully detwinned martensite was found after 300 °C/1000 cycles. After superelastic cycling at 400 °C (Fig. 5c) a distinctly different microstructure arises, i.e., hardly any dislocations were found after 1000 cycles.

In order to analyze the impact of cyclic deformation at different temperatures on the prevailing microstructures within the entire volume in more depth, neutron diffraction analyses were performed on fatigued single-crystalline $Co_{49}Ni_{21}Ga_{30}$ samples. For neutron analyses, the samples tested at 300 and 400 °C were selected, as the single cycle tests shown in Fig. 1 revealed similar stress hysteresis while cyclic tests showed a fundamentally different degradation behavior (Fig. 3a, b). From the neutron diffraction data measured at RT (Fig. 6), peak widths of {110} reflections of three sample-conditions were extracted: as-grown, fatigued at 300 °C/1000 cycles, and fatigued at 400 °C/100 cycles. The sample condition 400 °C/100 cycles was chosen for the peak width analysis due to the fact that no austenite remained in the microstructure at room temperature after cycling at 400 °C for 1000 cycles. Peak widths of the as-grown sample and the sample fatigued at 300 °C/1000 cycles were shown recently [30]. Note that the peaks of the 300 °C/1000 cycles condition were reevaluated and normalized to the sample dimensions, and thus, appear slightly different now. In Fig. 6, the widths of the 110 peaks of the three conditions are shown. After 300 °C/1000 cycles and 400 °C/100 cycles, the sample consists of two-phase composite crystals, i.e.,

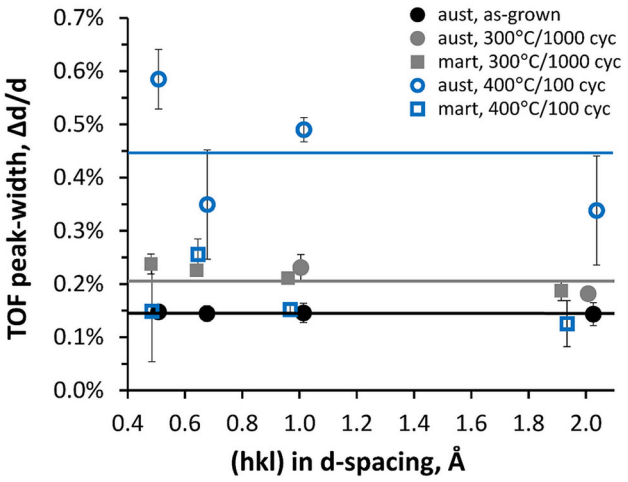

Fig. 7 Peak widths of hh0 peaks in TOF direction obtained by single-crystal Laue diffraction on backscattering detectors. TOF peak widths are given as $\Delta d/d$ (y-axis) plotted over the d-value of the corresponding Bragg reflection. The $\Delta d/d$ value corresponds to microstrain in units of %. Error bars are sometimes smaller than the symbols

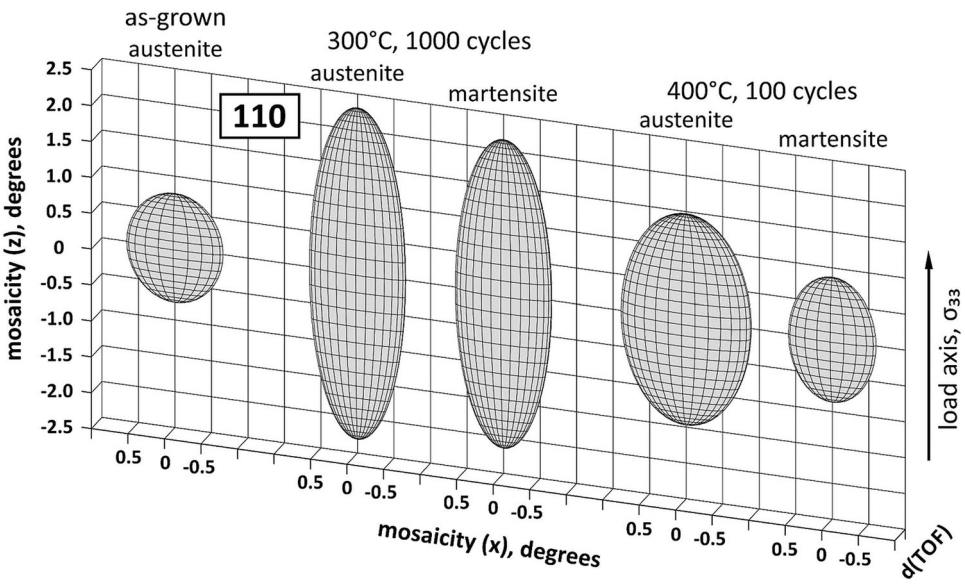

Fig. 6 Three-dimensional peak profile ellipsoids of 110 peaks obtained by single-crystal Laue diffraction on backscattering detectors. Samples fatigued at 300 °C/1000 cycles and 400 °C/100 cycles are composed of two-phase composite crystals of austenite and martensite, which show significant peak broadening. The peak profiles of the as-grown condition and after cycling at 300 °C are recompiled from [30]

stabilized martensite and residual austenite. The peak of the initial as-grown condition is slightly elongated as the sample shape is mapped onto the detector. Compared to the as-grown condition at 300 °C both austenite and martensite show a peak broadening of about 3.0° parallel to the load axis (z-detector coordinate), whereas perpendicular to the load direction (x-detector coordinate) no significant peak broadening can be observed. At 400 °C the martensite peaks are only slightly elongated whereas the austenite peaks are significantly broadened by about 1.8° parallel and by about 0.8° perpendicular to the load axis. As opposed to the 300 °C case, austenite peak broadening observed at 400 °C perpendicular to the load direction hints at a second defect-generating mechanism. Time-of-flight (TOF) peak widths are shown in Fig. 7: peak widths of the hh0 reflections were converted into units of Å and $\Delta d/d$ values are plotted against the mean d-value (d = lattice spacing) of their corresponding Bragg reflection, e.g., $(110)_{\text{austenite}} = 2.027$ Å, $(110)_{\text{martensite}} = 1.925$ Å. The TOF peak widths correspond to a deviation of the lattice spacing, Δd, from its mean value d. As they are also dependent on the wavelength, each hh0 set (i.e., 110, 220, 330, 440) is normalized by the mean d-value of its corresponding Bragg peak. The $\Delta d/d$ values obtained correspond to the microstrain of the single crystal in percent. Values for TOF peak widths of the as-grown austenite and 400 °C/100 cycles martensite yield about 0.15 %; the peak widths of 300 °C/1000 cycles austenite and 300 °C/1000 cycles martensite result in about 0.20 %. For 400 °C/100 cycles austenite, a value of about 0.45 % is obtained, cf. Figure 7. It is surprising that the as-grown austenite and 400 °C/100 cycles martensite are on a similar low microstrain level, whereas the 400 °C/100 cycles austenite shows significantly larger microstrain. At 300 °C, the low amount of 6 ± 2 vol% residual austenite is most probably interfaced with 94 ± 2 vol% stabilized martensite [30]; therefore, the microstrain levels of austenite and martensite are similar.

Figure 8 visualizes the occupation probability of Co, Ni, and Ga on the atomic sites 0,0,0 and 0.5,0.5,0.5 in (a) the as-grown B2 austenite and (b) the fatigued tetragonal martensite structure. In the as-grown austenite, chemical ordering with a preferred occupation of Co on 0,0,0 and Ni + Ga on 0.5,0.5,0.5 was observed. After fatigue at 400 °C/1000 cycles (corresponding to 8.5 h aging time), martensite is stabilized by chemical disorder, i.e., the atomic distribution is adapted to the external stress field enforcing the martensitic transformation (see also [32]). Reciprocal space sections directly obtained from neutron data in Fig. 8c, d are the basis for the structures shown in Fig. 8a, b, respectively. In Fig. 8c, weak and concomitantly sharp superlattice reflections of type $h + k + l = 2n + 1$, with $n = 0,1,2\ldots$ are present (white arrows) indicating B2-type ordering, whereas in Fig. 8d, superlattice reflections have become extremely weak. This clearly indicates the evolution of a tetragonal structure with a very low degree of order close to bct, i.e., with almost equal distributions of Co, Ni, and Ga on 0,0,0 and 0.5,0.5,0.5.

Discussion

The current experimental investigations clearly reveal that cyclic deformation of [001]-oriented Co–Ni–Ga single crystals under tensile loading conditions at elevated temperatures is not only dominated by dislocation-controlled degradation, but also by changes in the degree of chemical order induced by diffusion. The evolution of the stress hysteresis in single cycle tests under tension shown in Fig. 1a hints at changes in the prevalent transformation behavior induced by the increasing temperature. The stress hysteresis remains relatively constant following any temperature increase up to 200 °C. This is in good agreement with the results of Dadda et al. [15], who observed an almost constant stress hysteresis up to 150 °C for superelastic compression tests on single-crystalline [001]-oriented Co–Ni–Ga [15]. As tension–compression asymmetry affects variant selection [19, 30], differences in material behavior had to be expected. Further increase of temperature led to a significant increase in the width of the stress hysteresis up to 375 °C. Above 375 °C, the stress hysteresis starts to decrease until it reaches a value of 25 MPa again, which was also determined for a test temperature of 200 °C. The width of the stress hysteresis in general is affected by at least three factors in single-crystalline SMAs:

(1) The amount of dissipated energy due to frictional processes at the interphase and/or martensite intervariant boundaries inducing dislocations in the microstructure, which in turn pin the phase and variant boundaries [6].
(2) The degree of phase stability of the stress-induced low-temperature phase, which can be changed by diffusional processes such as precipitation and/or changes in the degree of chemical order, i.e., long- and/or short-range order [2, 8, 9, 26–28, 30–32, 35].
(3) A decrease of A_s due to the occurrence of detwinning and/or martensite reorientation [16]. Especially upon detwinning, which prevails during forward transformation, the back stress that was stored in the twinned martensite is removed [16]. As a result of the loss of back stresses being capable in aiding reverse transformation, A_s is shifted to lower values, which is manifested in an increased stress hysteresis.

All three effects are able to stabilize the martensitic phase upon repeated loading leading to a decrease of A_s. Since multi-martensite variant activation is supposed to

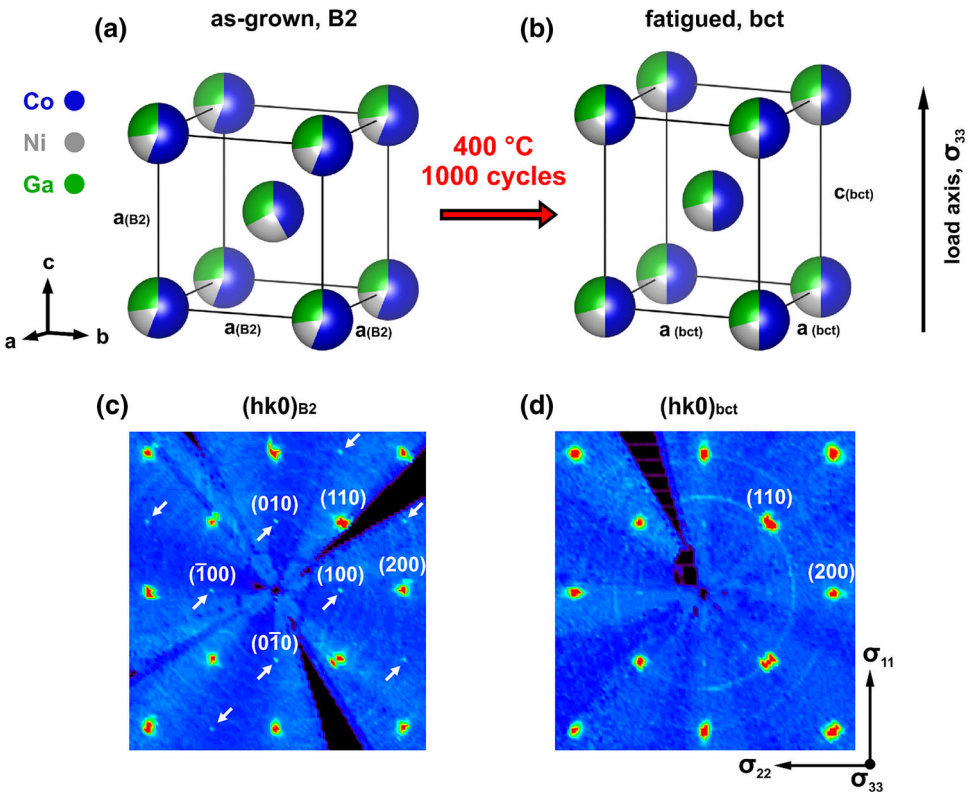

Fig. 8 The atomic order of Co–Ni–Ga crystals for **a** the initial as-grown B2-ordered austenite and **b** the body-centered martensite after fatigue at 400 °C/1000 cycles. The atomic distributions of Co, Ni, and Ga are different for the atomic sites (0,0,0) and (0.5,0.5,0.5): the distributions are unequal in **a** as indicated by the superstructure reflections (*white arrows*) in the corresponding diffractogram **c** (recompiled from [31]), whereas the structure in **b** shows an equal distribution of atoms according to a body-centered structure, thus, superstructure reflections are faded in **d**. σ_{11}, σ_{22}, and σ_{33} indicate the tensor components of the applied stress field

play a less important role in the current tensile tests [19, 30], the formation of dislocations at martensite inter-variant boundaries can be neglected. As the σ_{crit} for SIMT increases with the increasing test temperature according to the CC-relationship, the formation of dislocations at the austenite–martensite phase boundaries needs to be taken into account due to the development of high stresses exceeding the yield stress of the austenitic phase [15]. At elevated temperatures, diffusion cannot be neglected anymore and, thus, clearly should affect cyclic degradation in the Co–Ni–Ga single crystals. In addition, detwinning is markedly facilitated especially at higher temperatures, and has to be considered as well [16].

Single Cycle Tests

In order to shed light on the dominating elementary degradation mechanisms, the evolution of M_s and A_s temperatures are shown in Fig. 1b. Whereas the slope of M_s changes only marginally in the temperature regimes depicted, the alteration in the temperature dependence of A_s is significant. Note, that in general a decrease of σ_{crit} for austenite reverse transformation (A_s) correlates to the stabilization of the martensitic phase and vice versa. Stabilization in both cases might be due to diffusive and/or mechanical mechanisms [6, 29, 30]. The distinct decrease in A_s was also shown in a related study [30] for Co–Ni–Ga single crystals tested up to a maximum temperature of 400 °C for both, tension and compression loading [30]. In the current study, the evolution of A_s was analyzed up to 500 °C under tensile loads, which revealed an additional change in the temperature dependence of A_s above 400 °C. This is apparent from the comparison of the CC slopes in stages 1, 2 and 3, cf. Figure 1b. In general, the formation of defects due to interface friction at the austenite–martensite phase boundaries is supposed to result in the formation of irrecoverable strain and/or a decrease in σ_{crit}. As is well known, σ_{crit} correlates with M_s and the evolution of M_s for Co–Ni–Ga is shown in Fig. 1b. Clearly, temperature dependence of M_s in Fig. 1b exhibits a slight decrease to about 0.30 MPa/ °C visible in stage 2 followed by an increase to 0.44 MPa/ °C in stage 3. Since dislocation activity is known to be irreversible, this slight increase of the slope of dM_s/dT in stage 3 invalidates the argument of pronounced dislocation formation, as dM_s/dT seems to recover. T_m of the current Co–Ni–Ga alloy is about 1350 °C. Recovery processes are supposed to become significant above 0.4 T_m in conventional metallic alloys. Consequently, bulk recovery processes cannot be totally excluded under the current testing conditions, and, thus, small-scale dislocation rearrangement might occur, especially at 500 °C, i.e., at about 0.47 T_m. Thus, dislocations formed during superelastic loading might partially annihilate during unloading. This would clearly affect the stress

hysteresis leading to an increase of σ_{crit} for austenite (As) reverse transformation above 400 °C. This argumentation is in line with the slight decrease of dM_s/dT in stage 2 and the increase in stage 3, which is most obvious from Fig. 1b. The conclusion is further strengthened by the findings presented in [30], where multimartensite-variant activation under compression led to more pronounced dislocation activity and eventually a more pronounced decrease in dA_s/dT under compression than under tension in stage 2. Re-evaluating data from [30] it can be concluded that in general dislocation activity is enhanced at 300 °C. Thus, substantial changes in the microstructure have to occur above 400 °C in the single cycle tests in order to result in the observed decrease of the stress hysteresis (Fig. 1, stage 3). It seems to be reasonable, that diffusion of alloying elements, i.e., motion of individual atoms, is more favored than long range dislocation annihilation, i.e., concomitant motion of multiple atoms, in the single cycle tests due to low testing times. Thus, mainly diffusion is assumed to affect the change in the M_s- and A_s-temperature dependencies under the testing conditions given. The relatively steep increase in dA_s/dT in stage 3 hints at a diffusion triggered reordering mechanism, i.e., martensite stabilization due to changes in chemical order during forward transformation and reordering or rearrangement during unloading in the austenitic phase leading to a kind of austenite stabilization [29, 32]. Otsuka and Ren proposed the concept of symmetry-conforming short-range ordering (SC-SRO) for explanation of martensite phase stabilization and also discussed its high reversibility [32]. The influence of diffusion-controlled changes in the degree of chemical order on the transformation behavior of Co–Ni–Ga was recently demonstrated [29, 31]. Following different aging procedures, conducted in the stress-induced martensitic phase in Co–Ni–Ga single crystals, the degree of chemical order changed drastically from ordered to almost disordered [31]. In consequence, transformation temperatures significantly increased due to stabilization of the martensitic phase [29, 31]. Dadda el al. proposed that at elevated temperatures, the mobility of vacancies is significantly increased and, thus, enhanced diffusion facilitates the associated stabilization phenomenon (SC-SRO) as well as the interaction events at interphase or inter-variant boundaries [16]. Clearly, a further increase of the test temperature up to 500 °C in the current study leads to an increased contribution of diffusional processes. Here it is important to note that the SC-SRO concept focuses on symmetry-conforming changes in short-range order induced by point defects being present in generally small concentration [32]. Although experimental evidence provided in the current work solely reveals changes in long range order, the impact of SC-SRO cannot be fully excluded. Further studies have to be conducted, analyzing the role of density of defects, e.g., tailored by different quenching treatments, on stabilization and subsequent stability of martensite in Co–Ni–Ga. Above 400 °C, all mechanisms, which are leading to an increase in stress hysteresis, seem to diminish, and the initial width of the stress–strain hysteresis is restored. This leads to the conclusion that the aforementioned eased martensite detwinning at elevated temperatures appears not to be appropriate to explain the behavior in these tests (Fig. 1), at least at temperatures above 400 °C. According to the literature [16], detwinning generally is facilitated at elevated temperature, and, thus, should furthermore promote low A_s-temperatures. No microstructural evidence for regions containing twinned martensite was found in the microstructures of samples tested at 300 °C and above (cf. Figs. 4, 5, after fatigue testing). This leads to the conclusion that detwinning always is fully accomplished above a critical temperature. Above 400 °C, diffusion kinetics increase, leading to the enhanced activation of ordering mechanisms. Thus, it is most probable that diffusive rearrangement of the chemical order dominates the restoration of the stress hysteresis above 400 °C. The dislocations that formed in the very first cycles in the single cycle test (Fig. 1a) seem not to be highly influential. This can be deduced from the high reversibility shown for each single cycle in the range between 50 and 400 °C.

Cyclic Degradation

To discriminate the impacts of mechanical- and diffusion-controlled mechanisms on martensite stabilization and the cyclic transformation behavior, respectively, of Co–Ni–Ga single crystals, experiments at different temperatures were conducted. Figure 2 shows the results of the superelastic cycling experiment conducted at 400 °C. Comparing these results to data obtained from testing at 300 °C [30], it becomes apparent that the degradation behavior differs significantly at those temperatures, despite very similar hysteresis in the single cycle experiments (inset in Fig. 1a). Figure 3 depicts characteristic values taken from the cyclic deformation data. The alteration of σ_{crit} for SIMT ($\Delta\sigma_{crit}$ in Fig. 3a, which is known to represent a clear indicator for functional degradation [6, 36]) clearly illustrates a change in degradation behavior at about 300 °C. Whereas at 100 °C no change of $\Delta\sigma_{crit}$ was observed within 1000 cycles, at 300 °C $\Delta\sigma_{crit}$ for SIMT decreases by about 250 MPa. At 400 °C the decrease in $\Delta\sigma_{crit}$ is considerably less pronounced. This clearly indicates a change in the prevalent degradation mechanism. With respect to mechanical martensite stabilization, the stress fields around dislocations provide for intrinsic mechanical energy, capable in pinning of evolving martensite variants. At the same time, these internal stress fields also support the

martensitic transformation in the subsequent cycle [6, 36]. Diffusion-controlled martensite stabilization is supposed to proceed without any defect generation, resulting in its high reversibility [29, 32]. Keeping in mind that the single cycle test in Fig. 1 already revealed a potentially strong impact of diffusion on the shape of the stress–strain hysteresis, the decrease in $\Delta\sigma_{crit}$, which is less pronounced following cycling at 400 °C, indicates a minor impact of dislocation formation at this temperature. Figure 3b further strengthens this argument. Cycling at 300 °C resulted in rapid accumulation of permanent strain in the very first cycles indicating intensive dislocation formation. Further evolution of permanent strain indicates saturation. Considering cyclic deformation at 400 °C the almost linear slope of the permanent strain accumulation as a function of cycle number is supposed to be an indicator for a time-based degradation mechanism, i.e., diffusive aging phenomena affecting the transformation behavior as discussed in more detail in the subsequent chapters. Time dependent diffusive degradation was also observed in other HT-SMAs. In Ti–Ta(–Al) alloys the dwell time in a critical temperature range clearly affects the degradation behavior. Higher heating–cooling rates, corresponding to shorter dwell times, resulted in intensive dislocation activity, whereas lower heating–cooling rates (high dwell times in the critical temperature range) led to functional degradation induced by aging phenomena [26–28].

In order to allow for a qualitative evaluation of the contribution of each degradation mechanism to the overall degradation behavior in different temperature regimes, TEM and neutron diffraction analyses in differently fatigued conditions were conducted. Using the latter approach, peak profile broadening is a measure of single crystal perfection, i.e., peak broadening is induced by an increase in defect density. Peak profiles can be dissected to establish the correlation between peak broadening and specific defects such as point defects, stacking faults, dislocations, and single-crystal mosaic blocks. Each single crystal consists of smaller mosaic blocks that are slightly misoriented relative to each other and considerably contribute to peak broadening. When subjected to mechanical cycling, dislocation slip in mosaic blocks causes them to shear apart creating smaller mosaic blocks. Ungar et al. referred to mosaic blocks created by a controlled stress field as ‘cells’ with low dislocation density surrounded by ‘cell walls’ with high dislocation density [35]. Ungar’s work explains why in metals and alloys that are sheared by certain slip systems increased mosaicity correlates strongly with increased dislocation density. In the current study, peak widths are given as mosaicity in units of degrees. As the peak profiles are compared to a reference condition, the instrumental peak width was not subtracted. Conclusions on the defect density in the sample volume can be drawn based on a semiquantitative approach by comparison of the peak profiles, complementing the TEM results.

The TEM images in Fig. 5a–d reveal varying densities of dislocations being present in the microstructure. Whereas dislocation formation seems to appear in a more dominant fashion after 200 °C/1000 cycles and 300 °C/1000 cycles, hardly any dislocations can be seen after 400 °C/1000 cycles (Fig. 5c). In excellent agreement with the TEM analysis, the peak width analysis of neutron diffraction data following 300 °C/1000 cycles revealed at significant peak broadening in the austenite and martensite as discussed in Ref. [30]. Semiquantitative evaluation of the peak broadening in the sample cycled for 400 °C/100 cycles (Figs. 6, 7) also supports the findings obtained by TEM (Fig. 5c). Dislocation formation plays only a minor role during cyclic deformation at 400 °C in Co–Ni–Ga SMAs, even though peak broadening for the austenite is symmetrically enhanced following 400 °C/100 cycles as compared to the as-grown condition (Figs. 6, 7). By contrast, peak broadening for the martensitic phase following 400 °C/100 cycles remains fairly low (Figs. 6, 7). Although the peak width analysis is only shown for the sample cycled for 400 °C/100 cycles, the TEM micrograph shown in Fig. 5c, i.e., after 400 °C/1000 cycles, supports the interpretation of low dislocation activity at this temperature, since hardly any dislocations were found in the microstructure. The sample loaded at 400 °C for 1000 cycles shows a fully stabilized martensitic structure, and thus, a peak width analysis of the austenitic phase was not possible in this case. The low dislocation density is quite unexpected, since the σ_{crit} for SIMT increases with the increasing temperature according to the CC-relationship. Eventually, this should result in a more pronounced dislocation activity, particularly as the yield strength of austenite decreases likewise. The slight broadening of the austenite peak in the z-direction after 100 superelastic cycles at 400 °C indicates that the stresses at 400 °C might reach the yield strength of the parent phase. As the martensite peak seems not to be broadened with respect to the as-grown condition (Figs. 6, 7), dislocation formation in the martensite phase can be neglected for 400 °C/100 cycles. The austenite peak broadenings perpendicular to the load direction and along TOF-direction (Figs. 6, 7) could be caused by lattice strain at the austenite/martensite interface as well as point defects induced in B2-ordered austenite on its way to disordered bct martensite. Thus, it can be assumed that peak broadening at 400 °C has to be related to different mechanisms as compared to 300 °C.

The diffraction analyses shown in Fig. 4e–h unequivocally reveal that the increasing temperatures lead to changes in the degree of chemical ordering after cycling. An analysis of the superlattice reflections reveals that following 200 °C/1000 cycles and 300 °C/1000 cycles, the

stabilized martensite features $L1_0$ ordering. TEM investigations following cycling at 400 °C revealed that even after 100 cycles the stabilized martensitic microstructure is characterized by a lower degree of order, indicated by significant weakening of the superlattice reflections in Fig. 4g. Analysis of diffraction pattern indicates an almost fully bct structure. Disordering is even more pronounced after 400 °C/1000 cycles (Fig. 4h). Surprisingly, no formation of precipitates was observed in the sample area probed after cycling independent of testing temperature. In fact, recent findings showed that upon aging at 400 °C in the martensitic phase the degree of order changes, leading to pronounced martensite stabilization and an increase in transformation temperatures [29, 31]. In the work of Niendorf et al. [29], SIM-aging was performed at 300 °C for 8.5 h. As 1000 superelastic cycles amounted to about 8.5 h in the present study, a comparison of the different test procedures is reasonable. Picornell et al. [37] revealed that following aging at 212 °C in stress-induced martensite in Co–Ni–Ga, the martensite was stabilized after 8 h. [37]. Thus, changes in the degree of chemical order due to aging may also have an impact on the cyclic transformation behavior at lower temperatures even though the impact would be relatively small. This might be an adequate explanation for the fully martensitic microstructure at room temperature after cycling at 200 °C/1000 cycles (Figs. 4a, e). As determined by neutron diffraction analysis, heating of the samples (cycled at 200 °C and cycled at 400 °C) up to 500 °C (not shown here) led to an austenitic microstructure at room temperature, indicating a chemical reordering process as discussed in the previous subsection. Thus, cycling at 200 °C led to an increase in transformation temperatures due to aging-related phenomena [29]. As dislocation formation seems to be of minor importance with respect to the superelastic cyclic performance following 200 °C/1000 cycles, indicated by the absence of accumulation of permanent strain and a minor decrease in σ_{crit} during cycling, this conclusion is reasonable. Dislocation formation seems not to be solely a function of the number of cycles but also a function of the temperature. At 200 °C, very slight changes in the degree of order and minor dislocation formation seem to occur simultaneously, both having impact on the reversibility of the martensitic transformation. The samples cycled at 300 and 400 °C exhibit similar stress hysteresis, but are supposed to be dominated by different mechanisms responsible for martensite stabilization (i.e., mechanical or diffusive). Thus, it can be concluded that diffusion-controlled stabilization of martensite proceeds much faster at 400 °C than mechanical pinning due to dislocation formation. In other words, dislocation formation seems only to be significant following a higher number of cycles in temperature regimes, where diffusion kinetics remain fairly low, e.g., 300 °C. When diffusion becomes significant, e.g., at 400 °C, dislocation formation is almost fully suppressed, as cyclic phase transformation is strongly hampered in sample regions already being stabilized by diffusion. For superelastic tests performed at 400 °C, a reversible stress–strain response can be seen in cycle 1000 (Fig. 2) even if the TEM micrograph shown in Fig. 5c shows a fully martensitic microstructure. This contradiction can be explained based on the elementary degradation mechanism. TEM analysis have been conducted at room temperature. Due to the changes in chemical order, transformation temperatures are significantly increased as has been shown for Co–Ni–Ga samples aged in martensite [29]. Thus, at room temperature, the sample is assumed to be well below its M_f temperature.

From the data obtained in this study, principle considerations on the elementary fatigue mechanisms of Co–Ni–Ga HT-SMA can be deduced, which are summarized schematically in Fig. 9. Considering the results from Picornell et al. [37], the impact of diffusion-controlled mechanisms at 200 °C is not negligible, so that the very slight degradation within the temperature region from 100 to 250 °C in Fig. 9 is supposed to be induced by both, dislocation formation and changes in the degree of chemical order. Within the transition zone, i.e., between approximately 250 and 340 °C, a change in the dominant degradation mode is apparent from the TEM and neutron diffraction results shown in Figs. 4, 5 and 6. It should be noted that temperature ranges also will be affected by strain rate, as this value is linked to dwell times in austenite and martensite. At 300 °C mainly dislocation formation dominates cyclic degradation, since stresses for the SIMT increase according to the CC-relationship. A further

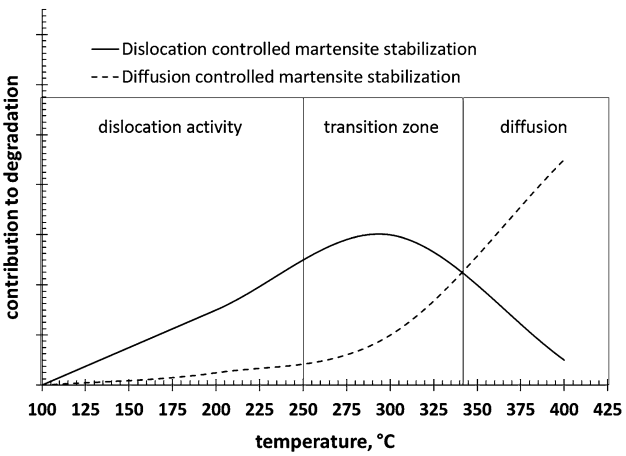

Fig. 9 Schematic illustrating the contribution of the two degradation mechanisms to the degradation of the superelastic performance of [001]-oriented Co–Ni–Ga shape memory single crystals during fatigue tests at different temperatures

increase in test temperature leads to a significant increase in the diffusive contribution and, thus, at 400 °C, martensite stabilization due to changes in the degree of chemical order governs cyclic degradation.

Conclusions

The present study revealed pronounced influence of the test temperature on the prevailing degradation mechanisms in a Co–Ni–Ga high-temperature shape memory alloy (HT-SMA). Cyclic loading experiments accompanied by TEM and neutron diffraction analyses helped to pinpoint the different elementary mechanisms and estimate their relative contribution to the overall degradation. The major findings can be summarized as follows:

(1) A distinct impact of the test temperature on the evolution of stress hysteresis during superelastic cycling of single-crystalline [001]-oriented Co–Ni–Ga HT-SMAs was found. Up to 225 °C, stress hysteresis remains relatively constant and subsequently starts to increase up to about 375 °C. Further increase in test temperature leads to decrease in stress hysteresis up to 500 °C.

(2) The governing degradation mechanism changes with increasing temperature from dislocation dominated to diffusion controlled. For the latter, changes in the degree of chemical order affect the shape of the stress–strain response.

(3) Using detailed TEM analyses and neutron diffraction, a qualitative evaluation of the contributions of both, dislocation-based and diffusion-controlled, degradation mechanisms on the overall cyclic stress–strain response was performed. Whereas up to 300 °C mainly dislocation activity governs cyclic degradation, above 375 °C a decrease in the degree of chemical order seems to constitute the major degradation mechanism.

Acknowledgments Financial supports by the Deutsche Forschungsgemeinschaft (DFG) within the Research Unit Program "Hochtemperatur-Formgedächtnislegierungen" (Contract Nos. NI1327/3-2; MA1175/34-2; SCHM 930/13-2 and SO505/2-2) and by the Tomsk State University Academic D.I. Mendeleev Fund Program are gratefully acknowledged.

References

1. Otsuka K, Wayman CM (eds) (1999) Shape memory materials. Cambridge University Press, Cambridge
2. Ma J, Karaman I, Noebe RD (2010) High temperature shape memory alloys. Int Mater Rev 55:257–315
3. Lagoudas D (ed) (2008) Shape memory alloys—modeling and engineering applications. Springer, New York
4. Morgan NB (2004) Medical shape memory alloy applications—the market and its products. Medical shape memory alloy applications—the market and its products. Mater Sci Eng A 378:16–23
5. Duerig TW, Melton KN, Stoeckel D, Wayman CM (1990) Engineering aspects of shape memory alloys. Butterworth-Heinemann, London
6. Krooß P, Somsen C, Niendorf T, Schaper M, Karaman I, Chumlyakov Y, Eggeler G, Maier HJ (2014) Cyclic degradation mechanisms in aged FeNiCoAlTa shape memory single crystals. Acta Mater 79:126–137
7. Krooß P, Holzweissig MJ, Niendorf T, Somsen C, Schaper M, Chumlyakov YI, Maier HJ (2014) Thermal cycling behavior of an aged FeNiCoAlTa single crystal shape memory alloy. Scripta Mater 81:28–31
8. Buenconsejo PJS, Kim HY, Hosoda H, Miyazaki S (2009) Shape memory behavior of Ti–Ta and its potential as a high-temperature shape memory alloy. Acta Mater 57:1068–1077
9. Buenconsejo PJS, Kim HY, Miyazaki S (2009) Effect of ternary alloying elements on the shape memory behavior of Ti–Ta alloys. Acta Mater 57:2509–2515
10. Hsieh SF, Wu SK (1998) A study on lattice parameters of martensite in Ti50.5-xNi49.5Zrx shape memory alloys. J Alloy Compd 270:237–241
11. Han XD, Zou WH, Wang R, Zhang Z, Yang DZ (1996) Structure and substructure of martensite in a Ti36.5Ni48.5Hf15 high temperature shape memory alloy. Acta Mater 44:3711–3721
12. König D, Zarnetta R, Savan A, Brunken H, Ludwig A (2011) Phase transformation, structural and functional fatigue properties of Ti-Ni-Hf shape memory thin films. Acta Mater 59:3267–3275
13. Xu Y, Shimizu S, Suzuki Y, Otsuka K, Ueki T, Mitose K (1997) Recovery and recrystallization processes in Ti–Pd–Ni high-temperature shape memory alloys. Acta Mater 45:1503–1511
14. Kovarik L, Yang F, Garg A, Diercks D, Kaufman M, Noebe RD, Mills MJ (2010) Structural analysis of a new precipitate phase in high-temperature TiNiPt shape memory alloys. Acta Mater 58:4660–4673
15. Dadda J, Maier HJ, Karaman I, Karaca HE, Chumlyakov YI (2006) Pseudoelasticity at elevated temperatures in [001] oriented Co49Ni21Ga30 single crystals under compression. Scripta Mater 55:663–666
16. Dadda J, Maier HJ, Karaman I, Karaca HE, Chumlyakov YI (2010) Tension—compression asymmetry in Co49Ni21Ga30 high-temperature shape memory alloy single crystals. Int J Mater Res 101:1503–1513
17. Dadda J, Maier HJ, Niklasch D, Karaman I, Karaca HE, Chumlyakov YI (2008) Pseudoelasticity and cyclic stability in Co49Ni21Ga30 shape-memory alloy single crystals at ambient temperature. Mater Trans A 39:2026–2039
18. Meyer D, Maier HJ, Dadda J, Karaman I, Karaca HE (2006) Thermally and stress-induced martensitic transformation in Co-Ni-Al ferromagnetic shape memory alloy single crystals. Mater Trans A 383–440:875–878
19. Niendorf T, Dadda J, Lackmann J, Monroe JA, Karaman I, Panchenko E, Karaca HE, Maier HJ (2013) Tension—compression asymmetry in Co49Ni21Ga30 high-temperature shape memory alloy single crystals. Mater Sci For 82:738–739
20. Kireeva IV, Picornell C, Pons J, Kretinina IV, Chumlyakov YI, Cesari E (2014) Effect of oriented γ precipitates on shape memory effect and superelasticity in Co–Ni–Ga single crystals. Acta Mater 68:127–139
21. Kireeva IV, Pons J, Picornell C, Chumlyakov YI, Cesari E, Kretinina IV (2013) Influence of γ nanometric particles on martensitic transformation and twinning structure of L10

martensite in CoeNieGa ferromagnetic shape memory single crystals. Intermetallics 35:60–66
22. Monroe JA, Karaman I, Karaca HE, Chumlyakov YI, Maier HJ (2010) High-temperature superelasticity and competing microstructural mechanisms in Co49Ni21Ga30 shape memory alloy single crystals under tension. Scripta Mater 62:368–371
23. Benafan O, Garg A, Noebe RD, Bigelow GS, Padula SA II, Gaydosh DJ, Schell N, Mabe JH, Vaidyanathan R (2014) Mechanical and functional behavior of a Ni-rich Ni50.3Ti 29.7Hf20 high temperature shape memory alloy. Intermetallics 50:94–107
24. Evirgen A, Karaman I, Santamarta R, Pons J, Noebe RD (2014) Microstructural characterization and superelastic response of a Ni 50.3Ti29.7Zr20 high-temperature shape memory alloy. Scripta Mater 81:12–15
25. Belbasi M, Salehi MT, Mousavi SAAA, Ebrahimi SM (2013) A study on the mechanical behavior and microstructure of NiTiHf shape memory alloy under hot deformation. Mater Sci Eng A 560:96–102
26. Niendorf T, Krooß P, Batyrsina E, Paulsen A, Frenzel J, Eggeler G, Maier HJ (2014) On the functional degradation of binary titanium-tantalum high-temperature shape memory alloys—a new concept for fatigue life extension. Funct Mater Lett 7:1450042
27. Niendorf T, Krooß P, Batyrsina E, Paulsen A, Motemani Y, Ludwig A, Buenconsejo P, Frenzel J, Eggeler G, Maier HJ (2014) Functional and structural fatigue of titanium tantalum high temperature shape memory alloys (HT SMAs). Mater Sci Eng A 620:359–366
28. Niendorf T, Krooß P, Somsen C, Rynko R, Paulsen A, Batyrsina E, Frenzel J, Eggeler G, Maier HJ (2015) Cyclic degradation of titanium-tantalum high-temperature shape memory alloys—the role of dislocation activity and chemical decomposition. Funct Mater Lett 8:1550062
29. Niendorf T, Krooß P, Somsen C, Eggeler G, Chumlyakov YI, Maier HJ (2015) Martensite aging—an avenue to new high temperature shape memory alloys. Acta Mater 89:298–304
30. Krooß P, Niendorf T, Kadletz PM, Somsen C, Gutmann MJ, Chumlyakov YI, Schmahl WW, Eggeler G, Maier HJ (2015) Functional fatigue and tension—compression asymmetry in [001]-oriented Co49Ni21Ga30 high-temperature shape memory alloy single crystals. Shape Memory Superelast 1:6–17
31. Kadletz PM, Krooß P, Chumlyakov YI, Gutmann MJ, Schmahl WW, Maier HJ, Niendorf T (2015) Martensite stabilization in shape memory alloys—experimental evidence for short-range ordering. Mater Lett 159:16–19
32. Ren X, Otsuka K (1997) Origin of rubber-like behavior in metal alloys. Nature 389:579–582
33. Keen DA, Gutmann MJ, Wilson CC (2006) SXD—the single-crystal diffractometer at the ISIS spallation neutron source. J Appl Cryst 39:714–722
34. Momma K, Izumi F (2011) VESTA 3 for three-dimensional visualization of crystal, volumetric and morphology data. J Appl Cryst 44:1272–1276
35. Ungar T, Mughrabi H, Rönnpagel D, Wilkens M (1984) X-ray line-broadening study of the dislocation cell structure in deformed [001]-orientated copper single crystals. Acta Metall 32:333–342
36. Gall K, Maier HJ (2002) Cyclic deformation mechanisms in precipitated NiTi shape memory alloys. Acta Mater 50: 4643–4657
37. Picornell C, Pons J, Cesari E, Chumlyakov YI, Dutkiewicz J (2009) Effect of aging under compressive stress along [100] in Co-Ni-Ga single crystals. Funct Mater Lett 2:83–86